Civil and Environmental Research
ISSN 2224-5790 (Paper) ISSN 2225-0514 (Online)
Vol.6, No.10, 2014
www.iiste.org

The Effect of Superplasticizer Type on Compression Failure of High–Strength Concrete

Chatarina Niken (corresponding author)[1*] Elly Tjahjono[1] Bambang Soegijono[2] Vera Indrawati[3]
1.Dept. of Civil Engineering, Indonesia University, Faculty of Technology, Depok, 16424, Indonesia
2.Laboratory of Advance Material, Faculty of Mathematical and sciences, University of Indonesia Depok 16424 Indonesia
3.Dept. of Research and Development, Indocement Ltd, Indonesia
* E-mail of the corresponding author: chatarinaniken@yahoo.com

The research is financed by University of Indonesia (Sponsoring information)

Abstract
Although superplasticizer has been used widely on buildings and bridge structures around the world, the concrete's behavior has not yet been understood well by civil engineers. The use of superplasticizer should guarantee that abnormal failure does not occur. This paper presents different compression failure types of cylindrical specimens using two kinds of superplasticizer based on experimental research for compression test of high strength concrete (HSC) with a minimum compressive strength of 60 MPa. Cylindrical specimens measuring 15 cm in diameter and 30 cm of high were used. Seven mixtures using H superplasticizer and 7 mixtures using V superplasticizer were used. Failure observations were conducted as compression load was applied until failure occured. There were two types of compression failure which were vertical and horizontal according to two types of FT-IR graphs of superplasticizer. FT-IR simple fingerprint of superplasticizer exhibited normal compressive failure, while complex fingerprint showed dangerous compressive failure.
Keywords: Superplasticizer, Compression failure, High-strength concrete, Fingerprint

1. Introduction

One of the important factors for compressive stress-strain curves of concrete is the localization of failure (Grassl & Jirasek 2006). Compression failure is the more important and dangerous mode of failure, as it is highly brittle and lacking ductility. Previous experiments suggested that the compression failure was actually caused by fractures (Bazant *et al*. 1997). Dynamic compression failure at high temperature has also been investigated (Li *et al*. 2012). The size effect is an effective way to calibrate the parameters of a fracture model which has been observed in previous researches (Bazant,& Yu 2009, Bazant 2000, Bazant *et al*. 1997, Jishan & Xixo 1990, Marti 1989). However, in normal-strength concrete beams that fail in compression, size effect on the strength was relatively small (Ozbolt *et al*. 2000). Modeling of concrete failure as combination of plasticity and damage has also investigated (Grassl & Jirasek 2006); and shear compression failure in deep beam has also been studied (Zararis,2003). Hussein and Marzouk 2000, published their study on the failure modes of HSC subjected to biaxial combination (compression-compression, compression-tension, tension-tension) while Hsu, 1993 and 1985 investigated compression with shear failure. The type of fracture can help determining the cause for the compressive strength of a tested cylinder being less than anticipated (ASTM 4.02, 2003).

Fracture in HSC tends to be characterized more accurately by linear elastic fracture mechanics than normal strength concrete. High strength concrete behaves more like a homogenous material, with its stress-strain curve being steeper, and remaining closer to linearity at a higher stress-strength ratio. The amount and degree of micro cracking in the interfacial transition zone (ITZ) between the cement paste matrix and the aggregates cause a more brittle mode of fracture and less volumetric dilation. Because of densely packed cement grains and reduced amount of pores and cracks, HSC has a stronger ITZ, which is due to a reduction in excess bleeding and filling of gaps by mineral admixtures (Nemati, *et al*. 1998). Concrete strength increases according to the decrease of the water to cement ratio. Superplasticizer addition to the concrete allows the reduction of the water to cement ratio and enables the production of high strength concrete.

Superplasticizers, also known as high range water reducers are chemical admixtures used where well-dispersed particle suspension is required. These polymers are used as dispersants to avoid particles segregation and to improve the flow characteristic in concrete applications. Conventional Polycarboxylate (PCEs) as superplasticizer are known to easily incorporate into the layer structure of clay by means of their pendant PEO side chains; hence their dispersing ability in concrete is much impeded by clay impurities (Lei & Plank, 2012). It was found that the effect of chemical structure on the paste fluidity was not significant at high w/c, they became significant at w/c below 25% (Yamada *et al*. 2000).

Liu *et al*. 2014, observed that the difference of superplasticizer type will change the amide structure and then change failure type of concrete and concrete performance. Polycarboxylate superplasticizer type, such as polycarboxylate surfactant, high early strength, for dry mix generate different failure type. However, the

working mechanism has not been fully understood, revealing in certain cases cement-superplasticizer incompatibilities. Therefore, additional superplasticizer should be studied to ensure normal failure.

2. Materials and Method

2.1. Materials

Ordinary Portland Cement (OPC) produced by Indocement Ltd was used. Condition of the aggregate was saturated surface dry (SSD). Fine aggregate in the form of river sand was brought from Sungai Liat (Bangka, Sumatra, Indonesia); specific gravity (SSD) was 2.6053; and absorption was 0.4%. The sand had been filtered and cleaned using a mixture of standard graphs obtained from the mid-gradation, according to ASTM C.33/C.33M-08. Coarse aggregate in the form of volcanic rock fragments was obtained from Banten, West Java, Indonesia. Composition of the coarse aggregate used was 70% size of 13-19mm; specific gravity (SSD) was 2.563; absorption was 1.543%; and 30% size of 6-12mm; specific gravity was 2.636; and absorption was 2.26%). Type F fly ash according to ASTM C618-8a was a waste material from the electrical power plant in Suralaya, West Java, Indonesia. In this mixture design, 0-15% fly ash replaced cement. Added material used was silicafume of 8-12% cement weight produced by Sika Indonesia Ltd. To achieve the desired high strength with low water to cementitious material ratio and good workability, two kinds polycarboxylic superplasticizer (V and H) under the commercial name Visco Crete from Sika Indonesia Ltd was added to the concrete mix as high range water reducer (HRWR). The dose of HRWR was less than 2% of the cement weight according to product recommendation. Local water was supplied by the Structure and Material Laboratory of University of Indonesia. An electrical scale was used especially for cementitious materials, superplasticizer, and water to obtain the accurate amount of water to cementitious material ratio.

Materials composition with superplasticizer V and H are displayed in Table 1 and Table 2 respectively.

Table 1. Composition of the mixture with superplasticizer V

Materials	V1	V2	V3	V4	V5	V6	V7
Cement (kg/m^3)	500	468.7	452.75	497	536.151	497	452.75
Silica fume (kg/m^3)	45	37.49	40	46.1	47.368	58	40
Fly ash (kg/m3)	0	70.3	56.25	0	66.612	0	56.25
Water (kg/m3)	154	154	144	141	170.526	139.95	144
Sand (kg/m3)	774.62	758.6	675.47	675.47	735.09	674.57	675.47
Coarse agregate (kg/m3)	774.62	758.6	857.53	857.53	933	858.43	857.53
6-12mm (30%)	232.4	227.6	257.26	257.26	279.9	257.53	257.26
13-20mm (70%)	542.2	531.03	600.27	600.27	653.1	600.9	600.27
HRWR	9	9	9	9	10.658	9	9

Table 2. Composition of the mixture with superplasticizer H

Materials	H1	H2	H3	H4	H5	H6	H7
Cement (kg/m^3)	**588.553**	**497**	**452.75**	**497**	**497**	**487**	**487**
Silica fume (kg/m^3)	**68.684**	**58**	**40**	**58**	**46.1**	**44**	**44**
Fly ash (kg/m3)	**0**	**0**	**56.25**	**0**	**0**	**8**	**8**
Water (kg/m3)	**165.73**	**139.95**	**144**	**145.5**	**141**	**140**	**140**
Sand (kg/m3)	**776.57**	**655.77**	**620.74**	**674.57**	**675.47**	**676.57**	**676.57**
Coarse agregate (kg/m3)	**988.24**	**834.51**	**787.87**	**858.43**	**857.53**	**857.53**	**857.53**
6-12mm (30%)	**296.47**	**250.35**	**236.36**	**257.53**	**257.26**	**257.26**	**257.26**
13-20mm (70%)	**691.77**	**584.16**	**551.51**	**600.9**	**600.27**	**600.27**	**600.27**
HRWR	**10.658**	**9**	**9**	**9**	**9**	**9**	**9**

2.2. Method

Ten cylinder specimens were made from each mixture composition. The specimens were cured after demoulding (one day after casting) by immersion in the water to the age of 7 days. Compression load was applied at ages of 28 and 56 days. Maximum load and failure types were noted. Outlying analysis according to ASTM C 178 was used to obtain the f'_c. Slump flow of every mixture was measured, and ratio between water and cementitious material, water and cement, sand and aggregate, cementitious material and aggregate were computed. Casting temperature and humidity were also recorded.

The structure of superplasticizer can be obtained by FT-IR spectra. For analysis, failure type, maximum load and superplasticizer structure and material ratio were compared.

3. Theory

3.1. Fracture mechanism

In 1969, Hatano presented a theory of failure in concrete. From ASTM C 39-03: standard test method for compressive strength of cylindrical concrete specimens shows five different types of fracture (Fig.1). This standard requires that report should include the type of fracture if other than the usual cone appears.

When neoprene caps are used, if requirements for perpendicularity of the cylinder ends or vertical

alignment during loading aren't met, load applied to the cylinder may be concentrated on one side of the specimen. This can cause a short shear failure similar to that shown in Fig. l (d), except that the failure plane intersects with the end of the cylinder. This type of fracture generally indicates the cylinder failed prematurely, yielding results lower than the actual strength of the concrete (Kosmatka *et al*. 2002)

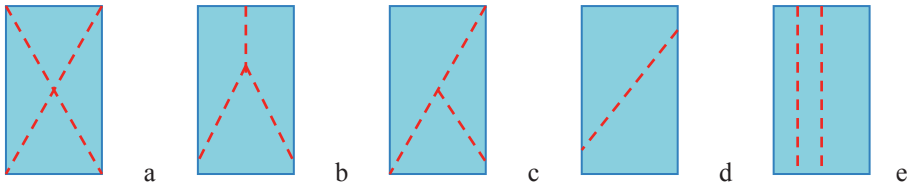

Figure 1. Types of fracture: (a). Cone, (b) Cone and split, (c) Cone and shear, (d) Shear, (e) Columnar

A cone failure happens when friction at the platens of the testing machine restraint lateral expansion of the concrete when the vertical compressive force is applied. This restraint confines the concrete near the platens and results in two relatively undamaged cones when the cylinder expand more laterally and exhibit a splitting failure similar to that shown in Fig. 1e. Such vertical splitting has been observed in numerous tests on high-strength specimens made of mortar or near cement paste, but the effect is less common in ordinary concrete when coarse aggregate is present (Neville 2003). ASTM 4.02, 2003 manual describes a case in which a fracture type that did not match any of those in Fig. 1 had been noted in a large number of tested cylinders. Crack parallel to the ends and at about mid height in the cylinder mode was taken as an indicator of not following standard testing procedures. A system of major continuous parallel cracks in the direction of compression may develop before the maximum compression load. These cracks are not axial splitting cracks but are produced by transverse tension. A system of parallel tensile cracks may be produced before the maximum load is reached in compression when a quasi-brittle material fails due to a compression loading combined with transverse tension, typical of shear failure.

The transverse tensile stress and the diagonal cracks caused by it have a large effect on the compression behavior in the direction of the cracks (Hsu 1988, 1993). The ASTM documents do not give any further information regarding causes of types of fracture other than the typical cone or whether any of the types shown are bad or good.

In quasi-brittle materials such as concrete, however, such ductile compression failure is possible only under lateral extremely high confining pressure; compression failure begins by the formation of axial splitting cracks. Lacking pressure lead the shear slip that cannot develop. The interlock of rough surfaces of cracks inclined to the principal compressive stress direction prevent any slip, unless the cracks are already widely opened and the material near the crack is heavily damaged.

The compression failure is caused predominantly by the release of stored energy from the structure, which commonly was influenced size effect. Type of compression failure that cannot be caused by any size effect occur when a global energy release is absent (Silva & Rodrigues, 2006, Bazant *et al*. 1997). A mechanism that does not cause global energy release is represented by the propagation of a continuous macroscopic splitting crack, while a transverse tensile crack causes a change in the macroscopic stress-field, and so it causes no global release energy.

There are three different mechanisms triggering compression fracture on the micro-scale, (Bazant *et al*. 1997):

1. Pores with micro-cracks
   It has long been known that porosity is the main controlling factor for compression strength of various materials. Axial cracks can grow from the pore only for a certain finite distance. This mechanism cannot explain the global fracture.
2. Inclusions with micro-cracks
   A rigid piece of stone aggregate in a softer mortar matrix (stiff inclusion), causes tensile stresses at a certain distance above and below the inclusion, which can produce short tensile splitting micro-cracks.
3. Wing-tip micro-cracks
   In a material without pores and without inclusions, cracks in a macroscopically uniform uniaxial compression field can be produced by weak inclined interfaces between crystals.

If the load required to drive the local mechanism of axial splitting crack propagation is higher than that required to drive the global mechanism of failure due to energy release, the global mechanism will occur.

3.2. Polycarboxylate Superplasticizer

The new generation of superplasticizer is based on polycarboxylate (PCE). In polycarboxylate superplasticizer,

amide synthesis process occurs (Liu *et al*. 2014). Amide is an organic compound containing $CONH_2$ or a compound with a metal replacing hydrogen in ammonia; or a group containing a carbonyl group linked to a nitrogen atom. Amide is derived from carboxylic acid and an amine. (Helmenstine 2014). Amide linkages in a biochemical context are called peptide bonds. Peptides have become instrumental in mass spectrometry, allowing the identification of protein of interest based on peptide masses and sequence (Liu *et al*. 2014). PCE-amide with the carboxyl amino ratio 4:1, exhibited the lowest surface tension, highest adsorption percentage, and the best paste fluidity result (Liu *et al*. 2014).

3.3. FT-IR

In the previous years the use of FT-IR to determine the structure of biological macromolecules has dramatically expanded. The new technique of FT-IR spectroscopy requires only small amounts of protein in a variety of environment. Therefore, high quality spectra can be obtained relatively easy without problems of background fluorescence, light scattering and problems related to the size of proteins. IR spectra may be obtained from samples in all phases (liquid, solid and gaseous). IR spectroscopy is the measurement of the wavelength and intensity of the absorption of infrared light by a sample (Griffiths & de Haseth, 2007). Wave number is the spatial frequency of a wave, either in cycles per unit distance or radians per unit distance. Photon energies associated with the part of the infrared may induce vibrational excitation of covalently bonded atoms and groups. The covalent bond in molecules are not rigid sticks but more like stiff springs that can be stretched and bend. Virtually all organics compounds will absorb infrared radiation that corresponds in energy to these vibrations. Vibrational modes are often given descriptive names, such as stretching, bending, scissoring, rocking and twisting. Exact frequency at which a given vibration occurs is determined by the strengths of the bonds and the mass of the component atoms. Furthermore, the number of observed absorptions may be decreased by molecular symmetry, spectrometer limitations, and spectroscopic selection rules. Reuch 2013, detected some general trends as follow:

1. Stretching frequencies are higher than corresponding bending frequencies. It is easier to bend a bond than to stretch or compress it;
2. Stretching frequencies in the bond of hydrogen is higher than those to heavier atoms;
3. Stretching frequencies of triple bond have higher than corresponding double bonds, which in turn have higher frequencies than single bond.

The complexity of this spectrum is typical of most infrared spectra, and it illustrates their use in identity substances. More energy is required to stretch or compress a bond than to bend it, and as it might be expected, the energy or frequency that characterizes the stretching vibration of a given bond is proportional to the bond dissociation energy. Equation 1 describes the major factors that influence the stretching frequency of a covalent bond between two atoms of mass m_1 and m_2. The force constant (f) is proportional to the strength of covalent bond m_1 and m_2. In the analog of a spring, it corresponds to the spring stiffness.

$$\nu = \frac{1}{2\pi c}\sqrt{\frac{f(m_1+m_2)}{m_1+m_2}} \quad (1)$$

$$k = \frac{2\pi}{\lambda} \quad (2)$$

Where:

υ: frequency in cm^{-1}, f,c: the force constant, c: the velocity of light
k: wave number , λ: wave length, V: speed of the wave,

Absorption spectroscopy is the absorption of radiation by its frequency or wavelength. The absorption occurs when energy is absorbed from the radiating field. Energy in infrared radiation corresponds to the energies involved in bond vibration. Absorptions also present functional groups (Smith 2003). Liu *et al*. 2014, reported a very high absorption of this sort means important things about the bonds in the compound. Different bond vibrates in a different way, involving different amounts of energy. FT-IR spectroscopy provides information about the secondary structure:

1. amide vibrations
2. amino acid side chain vibrations.

The IR spectra usually have sharp features that are characteristic of specific types of molecular vibration, making the spectra useful for sample identification. Absorption graph or finger print region can be used to identify an organic molecule (Clarc 2000) and the presence of a certain type of soft bond (Griffiths & de Haseth, 2007). The spectra reveal copolymer structure that can be used to characterize and analyze the superplasticizer (Ma 2010).

3.4. Cement Hydration

Hydration products growth can be seen in Fig.2 (Kurtis). The high rate of hydration product growth is started at the age of 7 days until 28 days.

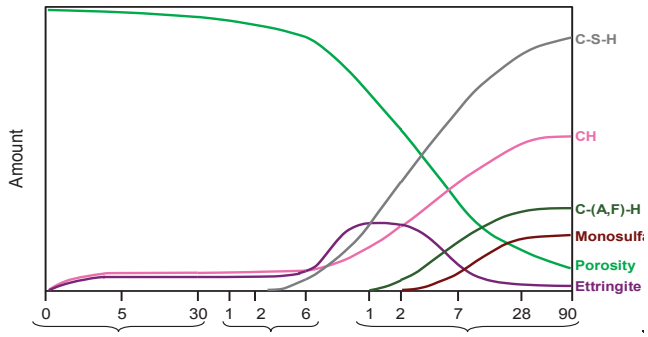

Fig.2. The growth of hydration product of ordinary Portland cement

At the age of 28 days and 56 days, hydration products such as CH, C-AF)-H, monosulfoaluminat and etrringite exhibited nearly constant value, in the other hand C-S-H showed a little faster growth. At the same time the amount of pores reached nearly constant value. At that time load-bearing volume fractions of hydrated cement ν(t) is more massive than before, according to product hydration growth. This fraction can grow continuously and significantly until many years as a result of progressive formation of bond among the solid particles of hydrated cement, than next bonds were formed in hydrated solid that is proved by polymerization of tricalcium silicate hydrates phenomenon in cement gel. The new bonds are formed continuously and occupy higher portion of the hydrated cement capable to carry load and can be counted as volume ν(t), while the solidified volume is not bonded densely yet cannot be as part of ν(t). ν(t) is formulated by equation 3 and 4. Equation 3 is associated with creep, and equation 4 is general form.

$$\nu(t) = \frac{F[\sigma(t)]}{\varepsilon^{v}(t)} \int_0^t \dot{\phi}\,(t - t')\, d\sigma(t') \qquad (3)$$

$$\frac{1}{\upsilon(t)} = \left(\frac{\lambda_0}{t}\right)^{m} + \alpha \qquad (4)$$

where $F[\sigma(t)]$: non dimentional function of cement stress, $\dot{\varepsilon}^{v}(t)$: rate of viscoelastic strain, $\dot{\phi}$: dϕ(t-t')/dt, ϕ: creep compliance, λ_o: empirical material constant, α: empirical constant.

The consequence of volume fraction growth (ν(t)) create stress of the solidified matter (hydrated cement) is associated with viscoelastic and viscous strain (Fig. 3) (Bazant et al, 1989).

Fig. 3. Solidification model in creep

4. Result

The results involved compression test, material ratio, casting environment and FT-IR.

4.1. Compression test

4.1.1 Compression stress

Compression test of the specimens at the ages of 28 and 56 days with superplasticizer V and H are shown in Table 3 and 4 respectively.

Table 3. Compression stress of specimens with superplasticizer V

Stress, MPa	V1	V2	V3	V4	V5	V6	V7
at 28 days (MPa)	50.09	59.48	61.64	57.68	67.31	62.09	61.64
at 56 days (MPa)	65.75	73.11	72.3	70.05	71.2	68.4	69.05

Table 4. Compression stress of specimens with superplasticizer H

Stress, MPa	H1	H2	H3	H4	H5	H6	H7
at 28 days (MPa)	66.82	66.82	67.31	62.09	62.13	73.04	68.93
at 56 days (MPa)	70.05	73.96	70.92	68.87	65.55	73.04	61.85

4.1.2. Compression failure type

Fig. 4. Compression failure type of specimens with superplasticizer V

Fig. 5. Compression failure type of specimens with superplasticizer H

4.2. Materials Ratio and Casting Temperature

Material ratio and casting environment with superplasticizer V and H, are displayed in Table 5 and 6 respectively.

Table 5. Material ratio and casting environment of specimens with superplasticizer V

Material rasio, environment	V1	V2	V3	V4	V5	V6	V7
HRWR/cement, for SCC 1-2%	1.8	1.92	1.99	1.81	1.99	1.81	1.99
HRWR/cememtitious (%)	1.65	1.56	1.64	1.66	1.64	1.62	1.64
Total aggregate	1549	1517	1533	1533	1668	1533	1533
Slump flow (cm)	77	70.5	65	57.5	53	58	61
Water/cemetitious	0.283	0.267	0.262	0.260	0.262	0.252	0.262
Sand/Coarse Aggregate	0.5	0.5	0.44	0.44	0.44	0.44	0.44
Cementitious/Aggregate	0.35	0.38	0.36	0.35	0.39	0.36	0.36
HRWR/cementitious (%)	1.65	1.56	1.64	1.66	1.64	1.62	1.64
Air content (%)				0.6	1.45	0.4	
water/cement	0.308	0.33	0.32	0.28	0.32	0.28	0.32
Silica/cement (%)	9	8.00	8.83	9.28	8.83	11.67	8.83
Fly ash /cement (%)	0	15.00	12.42	0	12.42	0	12.424
Fly ash/silica fume (%)	0	187.5	140.6	0	140.63	0	140.63
Casting temperature (^{o} C)	26.8	26	26.6	26.2	28	27.9	27.8
Casting humidity (%)	81	81	81	83	76	72	74

Table 6. Material ratio and casting environment of specimens with superplasticizer H

Material rasio, environment	H1	H2	H3	H4	H5	H6	H7
HRWR/cement, for SCC 1-2%	1.81	1.81	1.99	1.81	1.81	1.85	1.85
HRWR/cememtitious (%)	1.62	1.62	1.64	1.62	1.66	1.67	1.67
Total aggregate	1765	1490	1409	1533	1533	1534	1534
Slump flow (cm)	68	68	53.5	59.5	57.5	69	69
Water/cemetitious	0.252	0.252	0.262	0.262	0.260	0.260	0.260
Sand/Coarse Aggregate	0.44	0.44	0.44	0.44	0.44	0.44	0.44
Cementitious/Aggregate	0.37	0.37	0.39	0.36	0.35	0.35	0.35
HRWR/cementitious (%)	1.62	1.62	1.64	1.62	1.66	1.67	1.67
Air content (%)	1.48	1.48	1.45	0.4	1.9	0.5	0.7
water/cement	0.28	0.28	0.32	0.29	0.28	0.29	0.29
Silica/cement (%)	11.67	11.67	8.83	11.67	9.28	9.03	9.03
Fly ash /cement (%)	0	0	12.42	0	0	1.643	1.64
Fly ash/silica fume (%)	0	0	140.6	0	0	18.2	18.2
Casting temperature (^{o} C)	27.3	26.6	28	26	27.5	28.5	26.5
Casting humidity (%)	77	81	76	81	71	69	84

4.3. Fourier Transform-Infra Red (FT-IR)

Spectroscopy of Fourier transform-infra red of superplasticizer V and H are shown in Fig. 6.

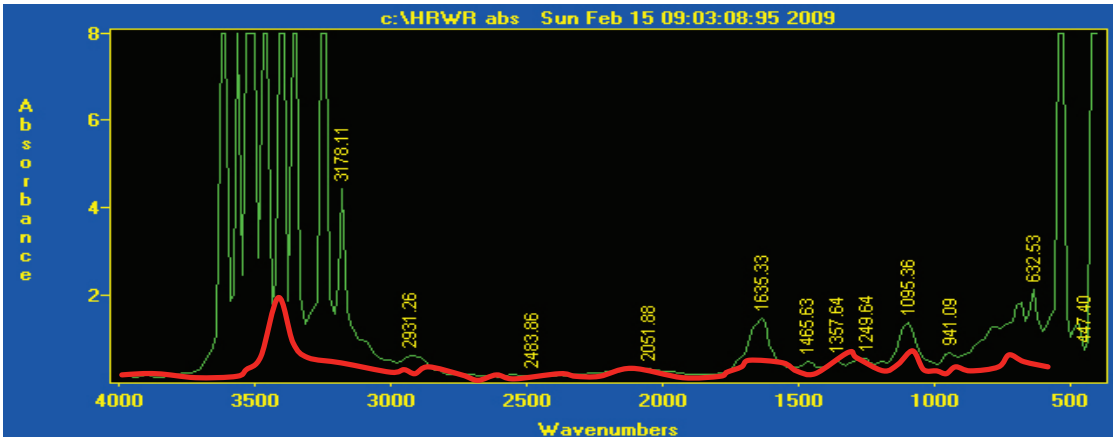

Superplasticizer V Superplasticizer H

Figure 6. FT-IR graph or fingerprint of superplasticizer V and H

Superplasticizer H (Figure 6), shows high intensity and high absorption at the wave number range of 3600-3200/cm. At the range, there are hydroxyl (bond O-H, with wave numbers 3610-3640 cm^{-1}), amines (bond N-H, with wave numbers 3300-3500 cm^{-1}), and aromatic rings which have bond of C-H, with wave numbers 3000-3100 cm^{-1} (Liu *et al*. 2014).

5. Discussion

All of the specimens exhibited compressive strength more than 60 MPa at the age of 56 days, but many specimens with superplasticizer H which were compression tested at the ages of 28 and 56 days, exhibited cracks horizontally (Fig.3), while specimens with superplasticizer V (Fig.2) show failure mode according to Fig. 1. Horizontal cracks suggests that the materials are very brittle; therefore, this cracks can make a structure not safe.

Materials ratio, as displayed in Table 5 and Table 6 does not show significant difference in value between specimens V and H; moreover, temperature and humidity at casting do not show significant difference.

The analysis of v(t) effect with viscoelastic strain ε^{v} is associated with hydration product growth (Fig.2), and related with the number and type of concrete ingredients (Eq.4). The solid hydration products give compression effect in the concrete microstructure which is balanced by capillary pores stress and response by disjoining pressure (Bazant et al, 1997). Superplasticizer in the mixture can change stress mechanism. The change is influenced by fingerprint of superplasticizer.

Fingerprints, as shown in Fig.4 between superplasticizer V and H, exhibit a different pattern. O-H, N-H and C-H bonds of superplasticizer H exhibit very complex bonds with many sharps; therefore, superplasticizer H contains specific bond, while superplasticizer V show very simple bond for all wave numbers. Correlation between bonds and wave number or wavelength is displayed in Figure 5 (Reuch 2013). Correlation between wavelength and wave number shown in Eq. 2

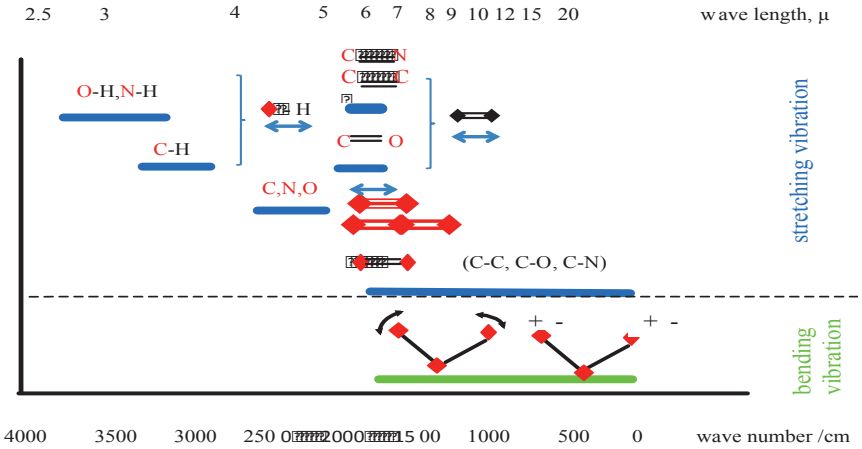

Figure 5. Correlation between bonds and wave number.

O-H, N-H, C-H are diatomic series with bond energies 102, 75, 81 respectively. The bond strength are even more scattered depending upon the structure of the rest of the molecule. O-H bond strengths vary from 90-119, N-H from 85-110 and C-H from 90 to 110 (k-cal/mol). O-H bond is polar covalent bond or polarity, which describes how equally bonding electrons are shared between atoms. A some what more sensitive parameter of bond strength is actually the bond length, short bond equal to stronger bond, but data on bond length in polyatomic molecules is much more scarce than bond energies because the detailed molecular structures are more difficult to obtain.

Fingerprints of superplasticizer H (Figure 4) exhibited a complex type, with high fluctuation of absorption with end sharp in the highest and lowest wave number range. If the assumption is that the molecule mass superplasticizer H is equal to superplasticizer V (according to Eq.1), thus the difference between fingerprint superplasticizer V and H is only on the constant of force. Therefore, bond stiffness between superplasticizer V and H has different properties. In the highest wave number, there are O-H, N-H and C-H bond, and only one mode of vibration occur that is stretching (Fig. 5). In this range, stretching and release of bond occur rapidly in superplasticizer H while in superplasticizer V, stretching and release happen smoothly. In the lowest wave number there are two modes of vibration: stretching and bending. Superplasticizer H exhibit high frequency absorption in the lowest wave number; therefore, stretching, bending and release of stretching and bending happened fast, while in superplasticizer V this phenomenon does not occur (Fig.5). Maximum absorption in superplasticizer V is about 25% absorption H, so the absorption of energy in superplasticizer V is smaller than in superplasticizer H. Therefore, energies involved in bond vibration is also smaller. There is no end sharp in superplasticizer V, suggest that there is no specific bond in superplasticizer V.

The solid hydration product reached about 90% since 28 age days; therefore the compression stress become higher. The integration of the compression stress, capillary pores stress, disjoining pressure in the one side (from concrete), and also stretching and bending vibration (from superplasticizer) with high fluctuation in the other side will lead the change of normal weak region (vertical) to abnormal weak region (horizontal); so that, compression failure to be horizontal.

This failure type should be avoided because it is very brittle and dangerous. The use of superplasticizer with simple fingers print of FT-IR is saver than superplasticizer with complex FT-IR fingerprint.

6. Conclusions

Conclusion from this research include the following:

1. The structural bond of superplasticizer determines compression failure type of concrete;
2. The influence of the use of superplasticizer on compression type is more than concrete composition variation;
3. The influence of the use of superplasticizer on compression type is more than temperature and humidity at casting time;
4. simplicity of FT-IR spectra or fingerprint (bond structure) of superplasticizer shows normally compressive failure;
5. complex FT-IR spectra or fingerprint (bond structure) of superplasticizer shown dangerous compressive failure
6. integration of the compression stress, capillary pores stress, disjoining pressure (from concrete) in the one side, and also stretching and bending vibration with high fluctuation (from superplasticizer) in the

other side will lead the change normal weak region from vertical to horizontal
7. specific molecules bond in superplasticizer lead to dangerous compressive failure

Acknowledgments
The authors would like to thank University of Indonesia (UI) for the financial support. Our special thanks are also extended to Indocement Ltd and Sika Indonesia Ltd for their full supports for discussion and materials. We are grateful to the technicians of Material and Structural Laboratory, and also Chemistry Laboratory of University of Indonesia for being helpfull during the experimental. Also special thanks for Language Institution of Indonesia University and my belove sun Hanindya Prasojo for language correction.

Reference
ASTM C33/C 33M-08, (2009), "Standard Specification for Concrete Aggregate", American Society for Testing and Materials, Vol 04.02, 12-22.
ASTM C 39-03, (2009), "Standard Test Method for Compressive Strength of Cylindrical Concrete Specimen", American Society for Testing and Materials, Vol 04.02, 23-29.
ASTM C618-8a, (2009). "Section: Construction, Concrete and Aggregates, Standard Specification for Coal Fly Ash and Raw or Calcined Natural Puzzolan for Use in Concrete", American Society for Testing and Materials, Vol 04.02, 331-333.
ASTM Standards Annual Book. (2003), Manual of Aggregate and Concrete Testing. Vol 4.02.
Bazant, Z.P.& Yu,Q. (2009), "Universal Size Effect Law and Effect of Crack Depth on Quasi-brittle Structure Strength", *Journal of Engineering Mechanics* February, ASCE, 78-84.
Bazant,Z.P. (2000), "Size Effect", *International Journal of Solids and Structures* 37, 69-80.
Bazant, Z.P., Fellow, ASCE & Xiang, Y. (1997), "Size Effect in Compression Fracture, Splitting Crack Band Propagation", *Journal of Engineering Mechanics* February, ASCE, 162-172.
Bažant, Z.P., Fellow, ASCE, and Prasannan, S. (1989), "Solidification Theory for Concrete Creep.I: Formulation", *J. Eng. Mech*.-ASCE 115.8 (1989) 1691-1703.
Clark, J. (2000), The Fingerprint Region of an Infrared Spectrum. www chemguide.
Grassl, P,& Jirasek, M. (2006), "Damage-Plastic Model for Concrete Failure", *International Journal of Solids and Structure* 43 (22-23), 7166-7196.
Griffiths,P.,& de Haseth, J.H.(2007), "*Fourier Transform Infrared Spectroscopy*", (2nd.ed). Wiley-Blackwell, 1-481.
Hatano. T. (1969), "Theory of Failure of Concrete and Similar Brittle Solid on the Basis of Strain", *International Journal of Fracture Mechanics* 5 (1), 73-79.
Heikal, M., Morsy, M.S. & Aiad, I.(2006), "Effect of Polycarboxylate Superplasticizer on Hydration Characteristics of Cement Pastes Containing Silicafume", *Ceramic-Silikaty*, 5-14.
Helmenstine, A.,M. (2014). Amine definition. About.com chemistry.
Hsu, T.T.C. (1985), "Softened Truss Model Theory for Shear and Torsion", *ACI Structural Journal* 6, 621-635.
Hsu, T.T.C. (1993), "Unified theory of Reinforced Concrete", CRC Press, Inc, Boca Raton, Fla.
Hussein, A.& Marzouk, H. (2000), "Behavior of High-Strength Concrete under Biaxial Stresses", *Materials Journal* 97 (1), 27-36.
Kosmatka, Kerkhoff & Panarese. (2002), "Design and Control of Concrete Mixtures", PCA.
Kurtis, K. Portland cement hydration. School of civil engineering, Georgia Institute of Technology, Atlanta, Georgia.
Lei, L.& Plank, J., (2012), "A Concept for a Polycarboxylate Superplasticizer Possessing Enhanced Clay Tolerance", *Journal Cement and Concrete Research* 42 (10), 1299-1306.
Liu, X., Wang, Z.& Li, H. (2014), "Synthesis, Characterization and Performance of a Polycarboxylate Superplasticizer with Amide Structure", *Colloids and surfaces A: Phycochemical and Engineering aspect* 448, 119-129.
Ma, X. (2010), "Synthesis of New Polyether Polycarboxylate Superplasticizer", *Journal of Wuhan University of Technology-Mater* 25 (5), Sci.Ed.,799-802.
Nemati, K.M., Monteiro, P.J.M.& Scivener, K.L. (1998), "Analysis of Compressive Stress-Induced Cracks in Concrete", *ACI Material Journal* 95, 617-630.
Neville, A., (2003)," *Properties of Concrete*, 4th Ed., Prentice Hall, England, 581-591.
Ozbolt, J., Meštrovic, D., Li, Y-J., & Eligehausen, R. (2000), "Compression Failure of Beams Made of Different Concrete Types and Sizes", *Journal of Structural Engineering* 126, 2, 200-209.
Reusch,W. (2013). www2.chemistry.msu.edu.
Silva, M.A.G., & Rodrigues, C.,C. (2006), "Size and Relative Stiffness Effects on Compressive Failure of Concrete Columns Wrapped with Glass FRP", *Journal of Materials in Civil Engineering*,18, 3, 334-342.
Smith, J.P. & Jinson-Smith, V. (2003), "The Endearing FT-IR Spectrophotometer", Anal Chem 75 1, 37-49.

Watanabe, K., Niwa, J., Yokota, H. & Iwanami, M. (2004), "Experimental Study on Stress-Strain Curve of Concrete Considering Localized Failure in Compression", *Journal of Advanced Concrete Technology* 2, 3, 395-407.

Yamada,K., Takahashi, T. & Matsuhisa, M., (2000), "Effect of the Chemical Structure on the Properties of Polycarboxylate-type Superplasticizer. *Journal Cement and Concrete Research* 30,20, 197-207.

Yi Li, Y., Tao, J., L., Gao, F. & Li, K. (2012), "Research on Dynamic Compressive Failure Criterion of Concrete at High Temperature", *Journal of Advanced Materials Research*, 446-449, 382-385

Zararis, P. (2003), Shear Compression Failure in Reinforced Concrete Deep Beams", *Journal of Structural Engineering* 129(4), 544–553.

The IISTE is a pioneer in the Open-Access hosting service and academic event management. The aim of the firm is Accelerating Global Knowledge Sharing.

More information about the firm can be found on the homepage:
http://www.iiste.org

CALL FOR JOURNAL PAPERS

There are more than 30 peer-reviewed academic journals hosted under the hosting platform.

Prospective authors of journals can find the submission instruction on the following page: http://www.iiste.org/journals/ All the journals articles are available online to the readers all over the world without financial, legal, or technical barriers other than those inseparable from gaining access to the internet itself. Paper version of the journals is also available upon request of readers and authors.

MORE RESOURCES

Book publication information: http://www.iiste.org/book/

IISTE Knowledge Sharing Partners

EBSCO, Index Copernicus, Ulrich's Periodicals Directory, JournalTOCS, PKP Open Archives Harvester, Bielefeld Academic Search Engine, Elektronische Zeitschriftenbibliothek EZB, Open J-Gate, OCLC WorldCat, Universe Digtial Library , NewJour, Google Scholar